Simulating turbulence in galactic halos and in the outer heliosphere

Journal of Physics: Conference Series **2997** (2025) 012001 doi:10.1088/1742-6596/2997/1/012001

Simulating turbulence in galactic halos and in the outer heliosphere

J Kleimann[1,2], S Oughton[3] and H Fichtner[1,2]

[1] Theoretische Physik IV, Ruhr-Universität Bochum, 44780 Bochum, Germany
[2] Ruhr Astroparticle and Plasma Physics Center (RAPP Center), 44780 Bochum, Germany
[3] Department of Mathematics, University of Waikato, Hamilton 3240, New Zealand

E-mail: jk@tp4.rub.de

Abstract. First, simulations of the wind-filled halos of starburst galaxies are performed in the framework of single-fluid magnetohydrodynamics, suitably extended to also track the self-consistent evolution of additional turbulence-related quantities. These quantities comprise the turbulent energy density, the cross-helicity, and the turbulent length scale. After a brief discussion of these extended equations and the employed numerical approach, we present selected simulation results, both for non-magnetized benchmark runs as well as for tests using the full system of equations. The dominant and unexpected feature of the former is a macroscopic flow instability near the rotational axis that prevents the outflow from reaching a steady state. Methods to determine the cause and nature of this instability are presented, followed by a preliminary analysis of the resulting turbulent properties. Second, the above framework is extended further to account for a non-constant energy difference (or residual energy), a quantity not conserved in the absence of dissipation, in addition to the Elsasser energies and by allowing each of these quantities its own characteristic correlation length scale. This setting is then applied to the outer heliosphere beyond the termination shock, where the solar wind expands both sub-Alfveńically and nonradially. The resulting solutions of this six-equation model are illustrated and studied in some detail.

1. Introduction

The study of plasma turbulence in the heliosphere (and elsewhere) is often faced with the problem of handling the enormous spatial and temporal range of scales which have to be bridged. Even with the much advanced computational resources which have become available in recent years, it is still not possible to perform direct numerical simulations resolving both the microscopic and macroscopic levels at the same time. In this situation, one viable alternative is to resort to Reynolds decomposition, whereby a quantity of interest X, typically the magnetic field $\mathbf{B}$ and the velocity $\mathbf{U}$, is decomposed according to $X = X_0 + x$ into its large-scale average $X_0 := \langle X \rangle$ and a small-scale fluctuation x. Reinserting these into the original hydrodynamic (HD) or magnetohydrodynamic (MHD) equations, one attains separate (though coupled) dynamic equations for $\partial_t X_0$ and $\partial_t x$ which can then be solved numerically on a coarse grid, provided that appropriate closure relations have been provided to account for the additional degrees of freedom. (The optional further inclusion of mass density ρ and its fluctuation as a third Reynolds-averaged pair of quantities, while in principle possible and interesting, is omitted from the present work and left for future studies.) For MHD, useful definitions for fluctuating quantities are, in terms

of Elsasser variables $\mathbf{z}^{\pm} := \mathbf{u} \pm \mathbf{b}/\sqrt{\rho}$,

$$Z^2 := \frac{\langle \mathbf{z}^+ \cdot \mathbf{z}^+ \rangle + \langle \mathbf{z}^- \cdot \mathbf{z}^- \rangle}{2} = \langle u^2 \rangle + \langle b^2/\rho \rangle \quad (1)$$

$$H_\mathsf{c} = \sigma_\mathsf{c}\, Z^2 := \frac{\langle \mathbf{z}^+ \cdot \mathbf{z}^+ \rangle - \langle \mathbf{z}^- \cdot \mathbf{z}^- \rangle}{2} = 2\, \langle \mathbf{u} \cdot \mathbf{b}/\sqrt{\rho} \rangle \quad (2)$$

$$D = \sigma_D\, Z^2 := \langle \mathbf{z}^+ \cdot \mathbf{z}^- \rangle = \langle u^2 \rangle - \langle b^2/\rho \rangle \quad (3)$$

for (twice) the turbulent total energy per unit mass (1), cross-helicity (2), and energy difference (3). Note that $|\sigma_{\mathrm{c},D}| \leq 1$ by definition.

In the simple(st) case of the so-called *three-equation model*, the turbulence is characterized by the three quantities Z^2, σ_c, and a correlation length scale λ, while the normalized energy difference is taken constant (e.g., Breech et al. [1] and references therein). A popular choice inspired by observational data from spacecraft [2, 3] is $\sigma_D = -1/3$, corresponding to $\langle b^2/\rho \rangle = 2\langle u^2 \rangle$. Alternatively, one may depart from this assumption, allowing $D \equiv \sigma_D\, Z^2$ to vary. Additionally using three (rather than one) separate length scales $\lambda_{\{\pm,D\}}$ for $Z^2_\pm \equiv Z^2(1 \pm \sigma_\mathsf{c})$ and D yields the aptly named *six-equation model*. The corresponding extended set of equations (not reproduced here, see Ref. [4] for an explicit list and antecendent references) admits a conservative form (plus several source terms), and can therefore be solved similarly to the usual MHD equations. One disadvantage is that, due to the phenomenological nature of closure, the equations themselves, even if implemented correctly, do not guarantee that $|\sigma_{\mathrm{c},D}| \leq 1$ remains true throughout a given simulation, and may therefore require corrective measures to enforce values exclusively within the permissible range.

The simulations of galactic halos to be presented in Section 2 will use a three-equation model on a simple 2D cylindrical grid, while Section 3 addresses the turbulence in the outer heliosphere using the full six-equation model on a nested 3D spherical grid. It should be noted that in both cases, the turbulence's back-reaction to the large-scale MHD variables is usually negligible.

2. Turbulence in galactic halos

2.1. Introductory remarks and motivation

Many galaxies are believed to host large-scale magnetized winds in their halos, the most likely driver of which is pressure from either starbursts or cosmic rays. The computation of cosmic-ray propagation in the halos of the Milky Way and other galaxies requires knowledge of, or at least constraints on, the corresponding diffusion tensor, which in turn depends on the amplitude of MHD fluctuations. Despite their general sophistication, contemporary numerical models of such winds do not include these turbulent fluctuations self-consistently. For this reason, we have started to incorporate a three-equation model of MHD turbulence into the galactic wind model to be discussed now. Since the focus is on the general structure of turbulence in a typical halo, we will start with a relatively simple setup, and leave its further refinement for future work.

2.2. Numerical setup

The Cronos code [5] is used to advance the equations of single-fluid ideal MHD on a 2D cylindrical grid of typically $(R, z) \in [0, 24]\,\mathrm{kpc} \times [-14, +14]\,\mathrm{kpc}$ with equidistant cell spacing, thereby assuming rotational symmetry around the z-axis. The only nonstandard addition is a source term representing a Miyamoto-Nagai gravity potential [6] for the disk, and optionally an additional spherical halo potential

$$\Phi_\mathrm{halo} = -\frac{GM_\mathrm{halo}}{R_\mathrm{b}} \left[\ln(1 + r/R_\mathrm{b}) + \frac{1}{1 + r/R_\mathrm{b}} \right] \quad (4)$$

based on Ref. [7] with $r = \sqrt{R^2 + z^2}$, $R_\mathrm{b} = 13\,\mathrm{kpc}$, and $M_\mathrm{halo} = 1.35 \cdot 10^{11} M_\odot$ (later to be replaced by the more recent Navarro-Frenk-White potential [8]). $M_\odot$ denotes the Sun's mass and G the gravitational constant. The effective mass of the disk (including the bulge component) is based on the Milky Way and amounts to $2.7 \cdot 10^{11}\,M_\odot$. The galaxy is represented through an oblate ellipsoidal surface of half-axes R_c and z_c, and all quantities except the magnetic field are kept fixed on this surface, with zero-gradient boundary conditions at the outer (non-axial) boundaries of the grid. Inside the ellipsoid, the poloidal velocity is set to zero, while the toroidal (φ-)component is set to the Keplerian velocity $U_\mathrm{Kep} = \sqrt{R\,\partial_R(\Phi_\mathrm{disk} + \Phi_\mathrm{halo})}$, which thus balances the total inward-pointing force of gravity.

Naively enforcing a custom magnetic field at the inner boundary by overwriting cells with their respective initial values would lead to a buildup of $(\nabla \cdot \mathbf{B})$-related errors that would quickly be advected into the rest of the computational domain. However, by specifically enforcing $U_R = U_z = 0$ inside the ellipsoid, it is ensured that the poloidal magnetic field therein remains equal to its initial configuration without incurring any violation of the solenoidality constraint, simply by virtue of the usual MHD induction equation. (Due to axial symmetry, the winding up of field lines caused by Keplerian rotation is immaterial to the divergence constraint.) Time integration is halted when a sufficiently steady state has been reached (or after it has become apparent that no such state will ever be reached, see Section 2.3).

2.3. An axial instability

As a first benchmark, the early galactic disk wind model by Habe & Ikeuchi [9] was chosen as a target. These authors numerically solved the HD equations on a 2D cylindrical grid, with Dirichlet boundary conditions on an annular $r \in [4, 12]\,\mathrm{kpc}$ disk located at the $z = 0$ boundary, and, for specific parameters, reported convergence towards a stationary wind solution after $\sim 200\,\mathrm{Ma}$ of physical time. However, attempts to reproduce their "wind-type model" steady-state solution instead led to a large-scale instability that would start as an inflow-dominated region near the z-axis at low distances from the disk and then quickly expand towards both z boundaries. A stable outflow was only obtained at larger distances from the rotational axis, with a very dynamic Kelvin-Helmholtz-type instability persisting at the interface between inflow and outflow regions, whose position continuously changes as the simulation advances in time.

Numerical artifacts relating to the coordinate singularity at $r = 0$ were excluded by reproducing the situation in a 3D Cartesian setting and obtaining identical results (to the extent possible given finite cell sizes). Additionally, several variations of the simulation have been conducted to identify the cause of the instability, some of which are illustrated in Figure 1. Notably, these included

(i) closing the central "hole" of the disk surface (as used by [9]) on which the galaxy's boundary conditions are specified,

(ii) disabling Keplerian rotation in favor of a completely static disk, and

(iii) significantly reducing the disk mass.

Option (i) did not prevent the instability from materializing itself but gave rise to a cylindrical sheet of downflowing material whose footpoints wandered radially along the disk. This phenomenon is probably an artifact of the $\mathbf{U} = \mathbf{0}$ boundary condition, while prescribing a nonzero value for the wind speed would have likely disconnected this feature from the disk. Option (ii) showed that without rotation, the inflow region remains restricted to the immediate vicinity of the z-axis, suggesting that it got dragged outwards by centrifugal forces in the rotating-disk case. A stable, stationary wind solution was finally obtained through a marked reduction in gravitational mass. Our preliminary conclusion is that the instability is an actual physical phenomenon, whose magnitude might however be exaggerated by zero-gradient boundary conditions at the upper and lower z boundaries, which can lead to a self-reinforcing

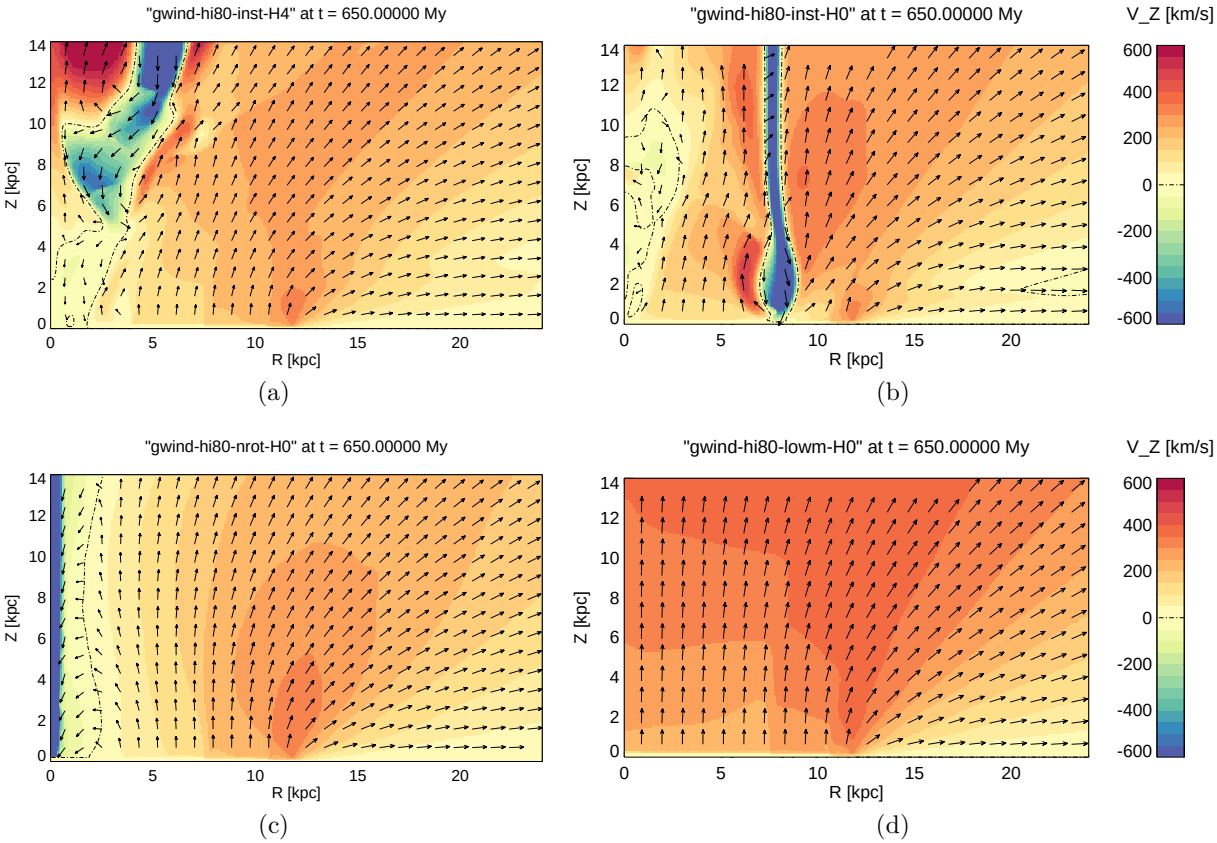

Figure 1. Contour plots of vertical velocity U_z (with vector arrows overplotted) for variations of the HD galactic wind simulation, taken at $t = 650$ Ma. (a): standard case, showing a pronounced hydrodynamic instability near the rotational axis. (b): like (a) but with the galactic disk extending up to the z-axis (thereby closing the central 4 kpc hole). (c): like (b) but without rotation. Note that the color bar has been capped at 600 km/s for improved visibility of finer structures. (d): like (b) but with the disk and halo masses both reduced to 10% of their original values.

feedback loop of ever-increasing inflow. (We refrain from implementing no-inflow condition here because it would a priori rule out any inflow whatsoever, even a physical one.) We therefore proceeded to focus on low-mass galaxies, leaving the further investigation of the instability and its physical causes to be addressed in the near future.

As to why this phenomenon was not seen in the simulations by Habe & Ikeuchi [9], one might speculate that the steady-state convergence reported by these authors was an artifact of stabilizing numerical diffusion due to their (by today's standards) very low spatial resolution of only 22×30 cells in total, but this hypothesis was easily disproved by follow-up simulations employing the same coarse resolution. More likely, their simulation was simply halted too early (after "only" 200 Ma) for the instability to fully develop.

2.4. First MHD runs with turbulence

The simulation setup described in the previous section is easily extended to magnetized environments with turbulence by amending the initial conditions through

(i) a poloidal magnetic field that is either homogeneous and purely vertical, or has field lines along hyperbolas (where the latter option has the advantage of the field being always normal

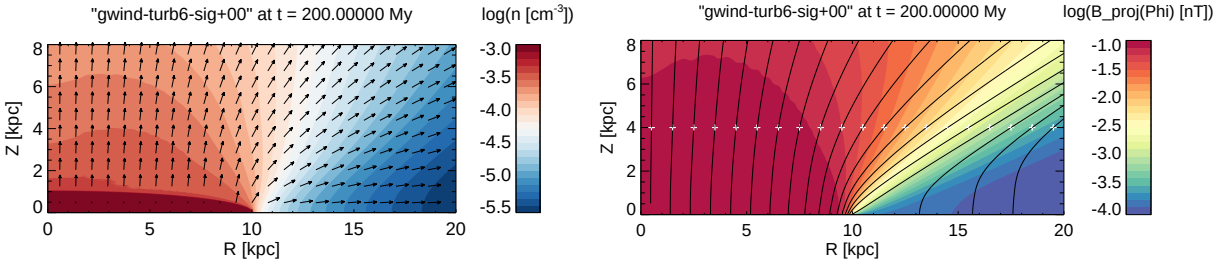

Figure 2. Converged galactic wind simulation for a low-mass galaxy. *Left:* contours of number density, with velocity arrows overplotted. *Right:* contours of magnetic field strength, with field lines overplotted. Note the logarithmic scale in both cases.

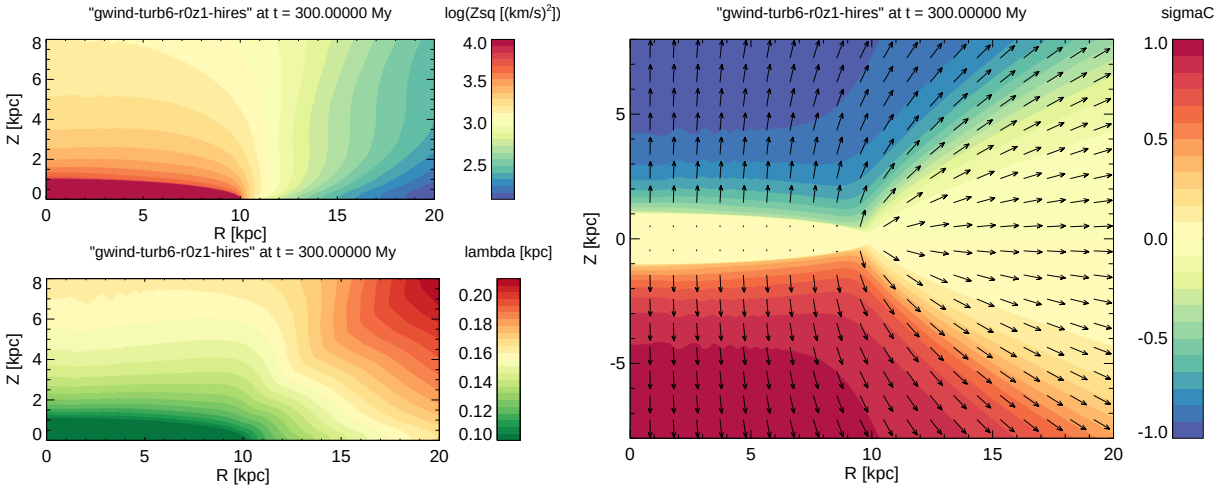

Figure 3. Turbulence quantities for the same situation as in Figure 2. *Top left:* turbulent energy density $\log(Z^2)$. *Bottom left:* correlation length scale λ. *Right:* normalized cross-helicity σ_c.

to the surface of the central ellipsoid for any ratio of half-axes, while the former is evidently much simpler to implement), and

(ii) spatially constant values (typically $Z^2 = 10^4\,(\mathrm{km/s})^2$, $\sigma_c = 0$, and $\lambda = 0.1\,\mathrm{kpc}$) for the turbulence-related quantities of the three-equation model.

Typical results from a converged run are shown in Figures 2 and 3. The characteristic magnetic "X-shape" often seen in astronomical observations (e.g. [10, 11]) forms trivially through field lines being dragged out by the wind flow into which they are "frozen." As can be seen, the turbulent energy density diminishes with distance from the galaxy in a way that reflects the imprint of the shape of the central object. It is also interesting to note that the bimodal distribution of cross-helicity forms self-consistently as a function of magnetic polarity in each half-space. With the spatial distributions of both $\mathbf{B}$ and $\{Z^2, \sigma_c, \lambda\}$ known, we may also deduce the cosmic-ray diffusion coefficient/tensor in the halo once a suitable value for σ_D has been found. The latter is a free parameter of the three-equation model, and little is known about its value in galactic halos. However, parameter studies (not shown here) suggest its influence on the other turbulent variables to be rather weak, making $\sigma_D = 0$ (corresponding to equipartition of turbulent energy) a defendable choice. These issues will be pursued in detail in a forthcoming paper.

3. Turbulence in the outer heliosphere

This section summarizes selected results from Kleimann et al. [4], to which the reader is referred for more details and supplementary information. Therein, an earlier single-fluid, three-equation turbulence MHD model of the inner heliosphere [12] was first generalized to the outer heliosphere (thereby including the interaction of the solar wind (SW) with the interstellar medium) and then generalized further to a six-equation model of turbulence.

3.1. Numerical setup

All simulations reported on in this section were again performed with the CRONOS code [5] using Sun-centered, 3D spherical grids. In order to be able to cover the entire radial domain from the coronal base (0.3 au) to the heliopause and beyond (~ 900 au), a nested grid arrangement was used: In a first SW-only simulation, the inner boundary condition was transported out to about 80 au. This simulation quickly converges (on the fluid-crossing timescale), and the resulting data on the outer boundary is then saved and fed into the inner boundary of a second, coarser grid covering the radial $[80, 900]$ au range. Additionally, each grid employs varying cell sizes $\Delta r \propto \exp(r)$ with a size ratio of $(\Delta r)_{\min}/(\Delta r)_{\max} \sim 20$ to make efficient use of the available computational resources. The inner coronal boundary conditions of our model consist of a static dipolar Parker spiral magnetic field, a bimodal solar wind (latitudinal variations in density, temperature, and radial speed), and turbulence parameters that exhibited a variation similar to the slow/fast wind dichotomy. The relative simplicity of these boundary conditions (no time dependence or inclusion of observational data) is justified by noting that the main focus of these investigations is on the principal structure of turbulence in the inner heliosheath (the region enclosed between the termination shock and the heliopause), rather than on reproducing specific observational in-situ data from spacecraft. For this reason, a comparatively coarse spatial resolution of typically $200 \times 60 \times 90$ cells in (r, ϑ, φ) was deemed sufficient for both grids.

3.2. Validation

The correct operation of the code and the model implementation is obviously both vital and nontrivial. Since the setting under investigation is much too complex for analytical test cases, we used the three-equation version of our model to reproduce a corresponding simulation by Usmanov et al. [13]. Although the latter is a four-fluid model (H^+, He^{2+}, neutral H, and pickup ions), reasonable agreement was obtained for most variables and in particular for the position of discontinuities (termination shock, heliopause, bow shock) when the characteristics of both approaches is accounted for. For instance, the mass density of the one-fluid model can only be expected (and was confirmed) to resemble the neutral density in the local interstellar medium (LISM) or the ionized density in the outer heliosphere, but not vice versa. For further details, including side-by-side comparisons for various large-scale and small-scale (turbulent) quantities, see Ref. [4].

3.3. The six-equation run

Figure 4 shows the contour plots of the three turbulence quantities Z^2, σ_c, and σ_D after steady-state convergence had been reached. A fair amount of substructure can be seen in all cases, clearly modulated by the termination shock and the heliopause. The LISM boundary conditions are poorly known and thus somewhat arbitrary; this can be justified considering that the focus of our investigation was on the inner heliosheath, which is not influenced by the properties of turbulence prevailing in the LISM. The values of σ_c can be seen to span the entire permissible interval $[-1, +1]$, and even required a moderate amount of clamping to avoid regions where values outside of this interval would have been attained. Not so for σ_D, for which no such treatment was needed, although a considerable range is covered as well. In particular, we see a pronounced departure from the standard value of $-1/3$ in spite of this being the initial condition

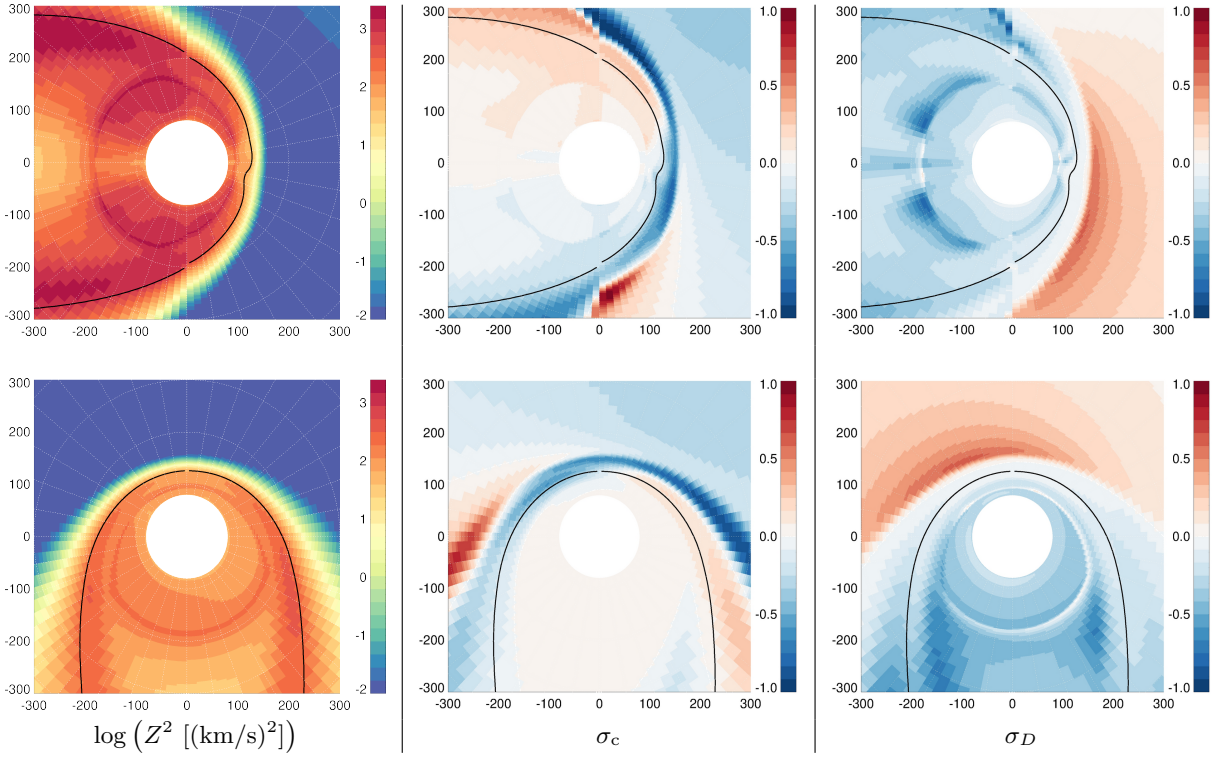

Figure 4. *Top row*: Contours of small-scale variables Z^2 (*left*), σ_c (*middle*), and σ_D (*right*) in the poloidal plane ($\varphi = 0°$) as computed on the outer grid. *Bottom row*: The same for the equatorial plane ($\vartheta = 90°$). All distances in au. In each plot, the thick black line marks the heliopause.

chosen for the SW region (but not for the LISM, which was initialized as $\sigma_D = 0$), particularly so near the heliopause (where $\sigma_D \approx 0$) and in the LISM (where positive values up to about 0.4 can be found).

4. Summary and conclusion

Firstly, a numerical one-fluid MHD model of incompressible ($\delta\rho = 0$) fluctuations is used to study the properties of turbulence in the magnetized, wind-filled halo of a typical disk galaxy. The numerical setup employed a single 2D cylindrical grid with equidistant cells, in which the galaxy is represented by an ellipsoid inside the computational volume. Attempts to verify the implementation using an earlier (purely hydrodynamic) reference work instead revealed the presence of an unexpected large-scale hydrodynamic instability near the rotational axis, whose occurrence could be linked to the galaxy's gravitating mass. Focusing on correspondingly low-mass galaxies, stationarity solutions for HD and MHD could be obtained including the small-scale quantities (turbulent energy density, cross-helicity, and correlation length scale). The study of the axial instability, which is likely relevant for Milky Way-sized galaxies, will be addressed in a future work.

Secondly, the above model was applied to study turbulent fluctuations and their transport in and interaction with the solar wind and the (inner) heliosheath. This required a slightly more intricate layout of two nested spherical 3D grids, in which the inner boundary conditions for the outer grid are found from the converged state on the inner (solar wind) grid. The three-equation version of this model has been verified through comparison with an existing four-

fluid model, showing reasonable agreement. The extended ("six-equation") model, in which the normalized turbulent energy difference (residual energy) σ_D is no longer a free parameter but can be calculated self-consistently, was then applied to study the same physical environment, with a particular focus on the inner heliosheath. The resulting distribution of σ_D revealed a striking and systematic deviation from the constant value $-1/3$ often assumed inside the termination shock.

Acknowledgments
JK thanks the organizers of the ASTRONUM 2024 conference for the invitation to present this work. Furthermore, financial support by the German Research Foundation (Deutsche Forschungsgemeinschaft, DFG) through project FI 706/23-1 and the Collaborative Research Center (Sonderforschungsbereich, SFB) 1491 is gratefully acknowledged.

References
[1] Breech B, Matthaeus W H, Minnie J, Bieber J W, Oughton S, Smith C W and Isenberg P A 2008 *J. Geophys. Res. (Space Phys.)* **113** A08105
[2] Matthaeus W H and Goldstein M L 1982 *J. Geophys. Res.* **87** 6011–6028
[3] Perri S and Balogh A 2010 *Geophys. Res. Lett.* **37** L17102
[4] Kleimann J, Oughton S, Fichtner H and Scherer K 2023 *Astron. Astrophys.* **953** 133
[5] Kissmann R, Kleimann J, Krebl B and Wiengarten T 2018 *Astron. Astrophys. Suppl. Ser.* **236** 53 (*Preprint* 1806.09479)
[6] Miyamoto M and Nagai R 1975 *Publ. Astron. Soc. Japan* **27** 533–543
[7] Innanen K A 1973 *Astrophys. Space Sci.* **22** 393–411
[8] Navarro J F, Frenk C S and White S D M 1997 *Astron. Astrophys.* **490** 493–508 (*Preprint* astro-ph/9611107)
[9] Habe A and Ikeuchi S 1980 *Progress of Theoretical Physics* **64** 1995–2008
[10] Heesen V, Krause M, Beck R and Dettmar R J 2009 *Astron. Astrophys.* **506** 1123–1135 (*Preprint* 0908.2985)
[11] Krause M, Irwin J, Schmidt P, Stein Y, Miskolczi A, Carolina Mora-Partiarroyo S, Wiegert T, Beck R, Stil J M, Heald G, Li J T, Damas-Segovia A, Vargas C J, Rand R J, West J, Walterbos R A M, Dettmar R J, English J and Woodfinden A 2020 *Astron. Astrophys.* **639** A112 (*Preprint* 2004.14383)
[12] Wiengarten T, Fichtner H, Kleimann J and Kissmann R 2015 *Astrophys. J.* **805** 155 (*Preprint* 1504.01858)
[13] Usmanov A V, Goldstein M L and Matthaeus W H 2016 *Astron. Astrophys.* **820** 17